Excitation Spectrum of Aluminum Acceptors in Diamond under Uniaxial Stress

P. A. CROWTHER, P. J. DEAN,* AND W. F. SHERMAN
Wheatstone Physics Laboratory, King's College, London, England
(Received 11 May 1966; revised manuscript received 1 August 1966)

A high-resolution survey of the 0.30–0.37-eV spectra, attributed to transitions at acceptor centers, obtained from several natural p-type semiconducting diamonds at 80°K, is presented. Effects on the spectrum of destruction of the normal site symmetry (T_d) by uniaxial compression are described. Hydrostatic stress has also been applied. Large spectral changes produced by uniaxial stress in the range 0–30 kbar have been analyzed in terms of the effective-mass theory of weakly bound electronic states, the lowest transitions being between quasihydrogenic s-p–like states. A *coupling scheme* here introduced for the p-like states is the *opposite* to that obtained for Si and Ge. Assignment of transitions has been made using theoretical band structures, results of reported spectral changes between 80 and 5°K, and the present stress spectra. Analysis of stress effects has been made using deformation-potential theory. The resulting potentials of $D_u^v = +2.47$, $D_u^v = +1.63$ eV are of the same sign as and similar magnitude to those of silicon.

1. INTRODUCTION

A SMALL percentage of natural diamonds exhibit a distinctive pale steel-blue color. These "II_b" crystals have low resistivity at 300°K, typically $\sim 300\ \Omega$ cm, compared with $\sim 10^{14}\ \Omega$ cm, for other types (the majority) and are strongly phosphorescent.[1] These effects are due to the presence of typically $\sim 5\times 10^{16}$ cm^{-3} acceptor centers, with partial compensation ($\sim 20\%$) by deep donors.

Early measurements showed that the thermal activation energy E_A of the acceptors is 0.36 ± 0.01 eV, and that II_b diamonds possess characteristic infrared absorption, the tail of which extends into the visible and is responsible for the observed color.[2,3]

A number of discrete absorption bands were observed at quantum energies between 0.30 and 0.37 eV; also a continuum with an ill-defined threshold near 0.37 eV.[3,4] This type of absorption spectrum is typical of that produced by photo-excitation of neutral acceptors.[5] The discrete bands are due to inter-bound-state excitations of the trapped hole, and the continuum is due to photo-ionization of the acceptor. The acceptor absorption spectrum is superimposed upon the broad intrinsic two- and three-phonon absorption present in all diamonds.[6,7]

Smith and Taylor studied the II_b spectrum,[8] and found that additional structure superimposed on the photo-ionization continuum may be interpreted as phonon replicas of the discrete absorption structure below 0.37 eV. This type of process is more probable in diamond than in silicon or germanium, because of the relatively compact hole wave functions in diamond.[9] *Single*-phonon absorption is induced at energies $\lesssim$ the Raman energy by the presence of acceptors.[8]

Studies of the temperature dependence of the acceptor spectrum show that there is considerable thermal broadening between 80 and 300°K and that below 80°K linewidths remain approximately constant at $\gtrsim 6\times 10^{-4}$ eV. The *intensities* of some absorption components decrease on cooling between 80 and 20°K, and are reduced essentially to zero at 5°K.[10,11]

Studies of edge luminescence, infrared optical absorption, and neutron-activation analysis have shown that the only neutral acceptor so far detected in natural diamond is due to substitutional aluminum.[12]

The diamond acceptor spectrum is more complicated than that of silicon and germanium, since the spin-orbit splitting of the valence-band edge is only 6 to 7 meV [12,13]—much less than E_A and comparable with kT at 80°K. There is a strong mixing of all three valence bands in the diamond acceptor wave functions, unlike the case of silicon, where the split-off valence band may be treated by perturbation theory.[14]

With the aim of elucidating information about the degeneracies and symmetries of the states involved,[15,16] the present work has included the examination of the

* Present address: Bell Telephone Laboratories, Murray Hill, New Jersey.

[1] J. F. H. Custers, Physica **18**, 489 (1952).
[2] P. T. Wedepohl, Proc. Phys. Soc. (London) **B70**, 177 (1957).
[3] I. G. Austin and R. Wolfe, Proc. Phys. Soc. (London) **B69**, 329 (1956).
[4] A. Halperin and J. Nahum, J. Phys. Chem. Solids **18**, 297 (1961).
[5] H. J. Hrostowski and R. H. Kaiser, J. Phys. Chem. Solids **4**, 148 (1958).
[6] C. D. Clark, R. W. Ditchburn, and H. B. Dyer, Proc. Roy. Soc. (London) **A237**, 75 (1956).
[7] J. R. Hardy and S. D. Smith, Phil. Mag. **6**, 1163 (1961).
[8] S. D. Smith and W. Taylor, Proc. Phys. Soc. (London) **79**, 1142 (1962).
[9] J. R. Hardy, Proc. Phys. Soc. (London) **79**, 1154 (1962).
[10] J. J. Charette, Physica **27**, 1061 (1961).
[11] J. R. Hardy, S. D. Smith, and W. Taylor, in *Proceedings of the International Conference on Semiconductor Physics, Exeter, 1962* (The Institute of Physics and the Physical Society, London, 1962), p. 521.
[12] P. J. Dean, E. C. Lightowlers, and D. R. Wight, Phys. Rev. **140**, A352 (1965).
[13] C. J. Rauch, in *Proceedings of the International Conference on Semiconductor Physics, Exeter, 1962* (The Institute of Physics and the Physical Society, London, 1962), p. 276.
[14] D. Schechter, J. Phys. Chem. Solids **23**, 237 (1962).
[15] W. Kohn, Solid State Phys. **5**, 257 (1957).
[16] R. H. Aggarwal and A. K. Ramdas, Phys. Rev. **137**, A602 (1965).

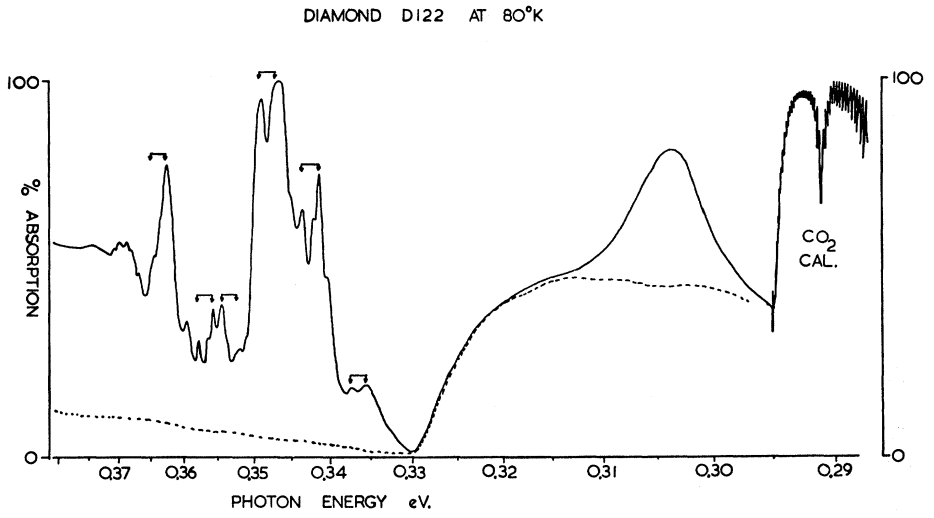

FIG. 1. The infrared absorption spectrum of a fairly typical type-II_b diamond. Transitions which appear, from thermal data, to involve the same excited state are shown by a pair of connected arrows; intrinsic lattice absorption, by a dashed line.

effect of uniaxial stress on the discrete bands of the acceptor spectrum.

2. EXPERIMENTAL DETAILS

Spectra were recorded using a double-pass double-beam monochromator equipped with a large LiF prism, and a liquid-nitrogen-cooled InSb photo-conductive detector (Mullard ORP13). The spectrometer had a maximum resolution of ~0.08 meV, but most of the spectra were recorded with resolution of 0.2–0.4 meV, which was adequate as the sharpest lines recorded had a width of 0.6 meV. Parallel plate stacks using silver chloride or selenium films were used to polarize the radiation as required.

Uniaxial pressure at 80°K was applied via the polished faces of two tungsten-carbide pistons within a precision-ground steel cylinder. The moving piston was driven by a relatively large-area hydraulic ram activated by externally applied oil pressure.[17,18]

The effect of *hydrostatic* pressure on both the acceptor spectrum and the intrinsic two-phonon absorption spectrum was also investigated using a modified type of Drickamer high-pressure apparatus.[19,17]

3. RESULTS

A. The Unperturbed Spectrum

Figure 1 shows the optical absorption spectrum of a typical natural II_b diamond in the range 0.30–0.37 eV. The broad hump in the region of 0.3 eV, which underlies the broad lowest acceptor transition at 0.3042 eV, is due to two-phonon lattice absorption. Apart from this, all the features in Fig. 1 are due to photoexcitation of the bound hole.

The spectrum is in fair agreement with that previously reported,[8] but careful examination of the energies of absorption peaks (Table I) suggests that previous values for most bands have been overestimated by 0.3 to 0.5 meV. The present spectra were carefully calibrated against gas lines using a continuous scan [Fig. 1], and the maximum error in the energies quoted in Table I is 0.03 meV unless otherwise stated.

The intense absorption in the region of 0.347 eV in the majority of II_b diamonds appears as a distorted single peak, as in Fig. 1. An exceptional specimen, which showed unusually narrow bandwidths over the whole range, did, however, show the 0.347-eV band clearly resolved into two components, as is shown in Fig. 2. The fact that large specimen-dependent low-temperature bandwidths are found in these spectra is probably caused by random strain in the specimens, the presence of which is evident from the prominent birefringence shown by II_b diamonds. It has also been shown that they contain high concentrations of edge dislocations,[20] which may be largely responsible for this strain.

Prominent absorption components in Fig. 1 are shown connected in pairs. For each pair the higher energy component increases in intensity on cooling from 80 to 5°K, whilst the lower energy components of each pair are all quenched at 5°K.[10,11] We believe, therefore, that the 2.1-meV splitting characteristic of all these pairs is a splitting of the acceptor ground state.

Combining these thermal data with results of the uniaxial stress experiments, it has been possible with the aid of effective-mass theory and energy-band theory to advance a plausible scheme of classification of acceptor hole states involved in the transitions up to

[17] W. F. Sherman, J. Sci. Instr. 43, 462 (1966).
[18] P. J. Dean and P. A. Crowther, in *Proceedings of the International Symposium on Radiative Recombination in Semiconductors* (Dunod Cie, Paris, 1965), p. 103.
[19] H. G. Drickamer, R. A. Fitch, and T. E. Slykhouse, J. Opt. Soc. Am. 47, 1015 (1957).
[20] E. R. Czerlinsky, A. D. Johnson, and G. H. Schwutte, in *Proceedings of the Industrial Diamond Symposium, Paris, 1962* (Industrial Distributors, London, 1963), p. 265.

TABLE I. Peak energies of the discrete absorption bands at 80°K.

Description[a]	Classification Thermal data	Thermal and stress data	Energy (eV) (present work)	Energy (eV) Smith and Taylor	Comment
SB	$A(1)''-2$ $A(1)'-2$	$\Gamma_8(g)$ $\Gamma_7(g)$ $-\Gamma_8(4)$ $\Gamma_6(4)$	0.3042±2	0.3046	Broad band
WB	$A(1)''-3$	$\Gamma_7(g)-\Gamma_8(3)$	0.3356±1	0.3360	
WB	$A(1)'-3$	$\Gamma_8(g)-\Gamma_8(3)$	0.3373±1	0.3377	
Sh	?	$\Gamma_7(g)-\Gamma_7(5)$	0.3404	0.3408	See Sec. 4 regarding selection rules.
SB	$A(1)''-4$	$\Gamma_7(g)-\Gamma_8(5)$	0.34148	0.3418	
Sh	?	$\Gamma_8(g)-\Gamma_7(5)$	0.34210	0.3425	Specimen-dependent resolution
SB	$A(1)'-4$	$\Gamma_8(g)-\Gamma_8(5)$	0.34353	0.3439	
WSh	?	$\Gamma_7(g)-\Gamma_6(1)$	0.3451	0.3456	
SB	?	$\Gamma_8(g)-\Gamma_7(2)$	0.34637	0.3473	Unresolved for many specimens (cf. Figs. 1 and 2).
SB	$A(1)''-5$	$\Gamma_7(g)-?$ $\Gamma_8(g)-\Gamma_6(1)$	0.34710		
Sh	?		0.34786		
SB	$A(1)'-5$		0.34913	0.3497	
Sh	?		0.34994		
WB	$A(1)''-6$		0.3524	0.3528	Very specimen-dependent half-width and height
SB	$A(1)'-6$		0.35456	0.3552	
SB	$A(1)''-7$		0.35579	0.3562	
	?		0.35641	0.3569	
SB	$A(1)'-7$		0.35789	0.3585	Very specimen-dependent half-width and height.
WB	?		0.35960	0.3599	
WB	?		0.36020		
SB	$A(1)''-8$		0.36273	0.3628	
WSh	?		0.3635	0.3643	
Sh	$A(1)'-8$		0.3646	0.3653	
WB	?		0.36685	0.3674	
Sh	?		0.36803		
WB	?		0.36883	0.3691	Specimen-dependent resolution in this in this region
WB	?		0.37002		
Sh	?		0.37068		

[a] Symbols: WB, weak band; SB, strong band or well-resolved band; Sh, well-defined "shoulder" on stronger band; WSh, weak ill-defined shoulder on stronger band. Column 2 refers to classification of transitions through thermal data alone. Ground states are denoted by $A(1)'$, $A(1)''$, excited states by 1–5. The weak band at 0.268 eV, described in Ref. 13, is omitted from this table, as it has not been observed in spectra from natural type-IIb diamonds. The optically active excited states are labeled in order of their energy relative to the ground state.

~0.35 eV. This scheme is included in Table I, and is discussed in Sec. 4.

B. Effects of Uniaxial Stress—0.30–0.37 eV Spectrum

Notwithstanding its anomalously great bandwidth—5.5 meV at 80°K—the 0.3042-eV transition under stress exhibits considerable dichroism and splitting, shown in Fig. (3). The large dichroism of the split band under ⟨001⟩ stress does *not* appear to be mainly due to thermal population effects between the split ground levels, since a comparison experiment at 300°K showed very similar dichroism, too large to be explained as a population effect at 300°K. It is thought that this large intrinsic effect is evidence that transition moments are extremely sensitive to the effective Bohr radii of the states involved, which are changed by the application of stress.

The behavior of the 0.3042-eV band under ⟨111⟩ stress is qualitatively similar to that of the ⟨001⟩ case, except that smaller splittings are obtained, and much smaller dichroism induced. For ⟨110⟩ compression, effects are again somewhat similar, except that at least *two* components are visible for $\mathbf{E}\|\chi$, where χ is the uniaxial stress, and the $\mathbf{E}\perp\chi$ component now anomalously shows almost zero shift with pressure. The higher

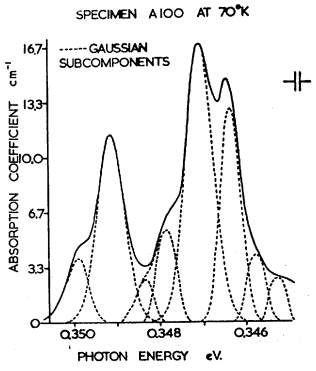

FIG. 2. Part of the absorption spectrum at 70°K of an exceptionally good specimen. The dotted lines show a possible analysis of the spectra into Gaussian subcomponents.

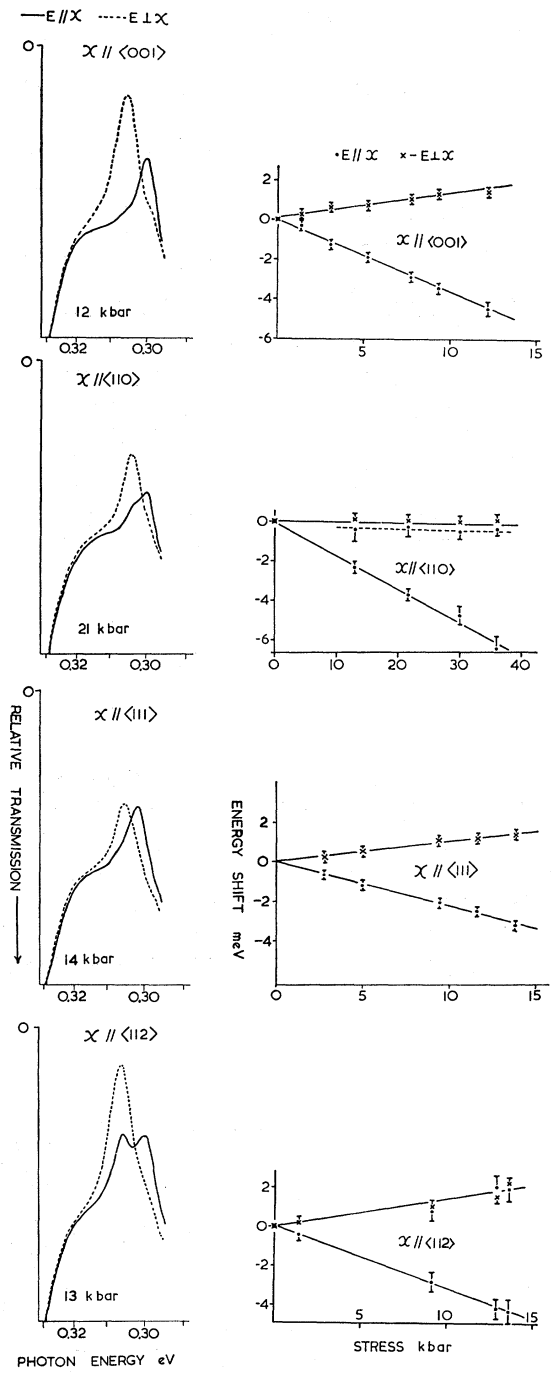

FIG. 3. The effect of uniaxial compression on the $A(1)$-2 band for different stress directions. Solid line denotes electric vector $\mathbf{E}\|\chi$, dotted line denotes $\mathbf{E}\perp\chi$. Note that the $A(1)$-2 acceptor transition is superimposed upon the broad 2-phonon intrinsic absorption.

energy $\mathbf{E}\|\chi$ component, although weak at lower stress, becomes very strong at 30 kbar, largely at the expense of the other $\mathbf{E}\|\chi$ component.

The effect of uniaxial stress on the remainder of the acceptor spectrum below 0.37 eV is very complicated (Figs. 4–7). The general effect for ⟨001⟩ compression is shown in Fig. 4, and is as follows. At low stresses, several bands show clearly defined splittings. By 6 kbar some of these low-stress splittings become hard to follow, and there is a general merging together of several components derived from different energies at zero stress. The large changes in intensity and nonlinearity of shift shown by many components is firm evidence that strong mixing of wave functions is occurring at these intermediate stresses. At still higher stresses, the confusion of the spectrum induced in this way diminishes, and to a large extent it may be seen that the resulting components regain *linear* shift rates, although the extrapolated intercepts of these linear shifts do not usually coincide with actual energies of peaks at zero stress. These effects are taken as evidence that for many of the states involved, complete *recoupling* of states has taken place by 13 kbar under ⟨001⟩ stress. Owing to the confusion at intermediate stress, it is occasionally difficult to be certain from which low-stress component a given high-stress component derives. Quantitative measurements for the ⟨001⟩ spectra are contained in Table V, where a theoretical interpretation of the stress effects is also summarized and compared.

Under ⟨111⟩ compression, the effect of stress on the higher transitions is seen to be weaker than under ⟨001⟩ stress, and recoupling, although present, is far from complete at the highest stress attained. Spectra were recorded at stress in excess of 15 kbar for ⟨110⟩ compression alone (Fig. 6). In the latter there is a simplification at high stress partly due to changes in intensity sufficient to extinguish some components under stress.

C. Effects of Uniaxial Stress—Phonon-Assisted Transitions

The absorption component at ~0.5 eV identified with single-phonon-assisted inter-bound-state acceptor transitions[8] was also examined under stress (Fig. 5). Additional structure appeared on the high-energy side of the zero-stress band for $\mathbf{E}\|\chi$, but not for $\mathbf{E}\perp\chi$, where χ is the uniaxial stress. Stress-induced phonon-assisted components are labeled P_1, P_2, P_3, and plausible corresponding zero-phonon components by Z_1, Z_2, Z_3. The relevant phonon energies derived in this way are given in Table II, upon examination of which it is evident that the phonon energies involved in different components under stress are not identical, and that there is a general reduction of the relevant phonon energy under uniaxial compression. The phonon values given in Table II for the zero-stress spectra are in reasonable agreement with those of Smith and Taylor. The P_3 phonon replicas are induced by uniaxial stress: They are invisible in the absence of stress, although Z_3 is prominent at zero stress.

TABLE II. Analysis of phonon-assisted transitions under uniaxial stress at 90°K.

Stress	Energy of phonon-assisted peak (eV)[a]	Energy of zero-phonon peak (eV)[a]	Phonon energy (eV)
0 kbar	0.5071±0.0003 0.6658±0.0010 0.8244±0.0020	0.3479±0.0001	0.1592±0.0003 (0.1589±0.0005)×2 (0.1588±0.0010)×3
	0.5029±0.0015	0.3430±0.0001	0.1599±0.0015
	0.4611±0.0004 0.6196±0.0010	0.3042±0.0001	0.1569±0.0005 (0.1577±0.0005)×2
⟨100⟩12 kbar $E\|\|\chi$	P_1 0.5021±0.0005	Z_1 0.3486±0.0002	0.1535±0.0007
	P_2 0.5089±0.0010	Z_2 0.3535±0.0005	0.1554±0.0015
	P_3 0.5156±0.0005	Z_3 0.3630±0.0002	0.1526±0.0007
⟨100⟩12 kbar $E\perp\chi$	0.5051±0.0005	0.3500±0.0002	0.1551±0.0007
⟨112⟩15 kbar $E\|\|\chi$	P_1 0.5038±0.0005	Z_1 0.3502±0.0005	0.1536±0.0010
	P_2 0.5102±0.0010	Z_2 0.3569±0.0002	0.1533±0.0012
	P_3 0.5176±0.0005	Z_3 0.3633±0.0002	0.1543±0.0007
⟨112⟩15 kbar $E\perp\chi$	P_1 0.5021±0.0010	Z_1 0.3466±0.0002	0.1555±0.0012
	P_2 0.5071±0.0005	Z_2 0.3515±0.0002	0.1556±0.0007
	P_3 0.5108±0.0010	Z_3 0.3571±0.0002	0.1537±0.0012
⟨110⟩22 kbar $E\|\|\chi$	P_1 0.5033±0.0005	Z_1 0.3587±0.0002	0.1546±0.0007
	P_2 0.5095±0.0010	Z_2 0.3540±0.0005	0.1555±0.0015
	P_3 0.5170±0.0005	Z_3 0.3620±0.0002	0.1550±0.0007
⟨110⟩22 kbar $E\perp\chi$	0.5053±0.0005	0.3492±0.0002	0.1561±0.0007

[a] The symbols Z_1, Z_2, Z_3 and P_1, P_2, P_3 refer to the components labeled in Fig. 4, and represent zero-phonon (i.e., no-phonon) and one-phonon-assisted inter–bound-state excitations of the hole at the aluminum acceptor center.

D. Effects of Hydrostatic Stress

Within the experimental limitations, no effect upon the acceptor spectrum between 0.30 and 0.37 eV was detected under the application of hydrostatic pressure up to 40 kbar. This is in accord with theoretical expectations for bound-hole–bound-hole transitions (Sec. 4B).

A prominent peak at 0.2679 eV in the two-phonon intrinsic lattice absorption remained sharp under hydrostatic pressure, and shifted linearly up to 40-kbar pressure. This peak represents the sum of transverse optic (TO) plus longitudinal acoustic (LA) phonon energies at the ⟨111⟩ first zero boundary.[21] The shift rate was $+7\times10^{-8}$ eV bar^{-1}, which implies that 260-

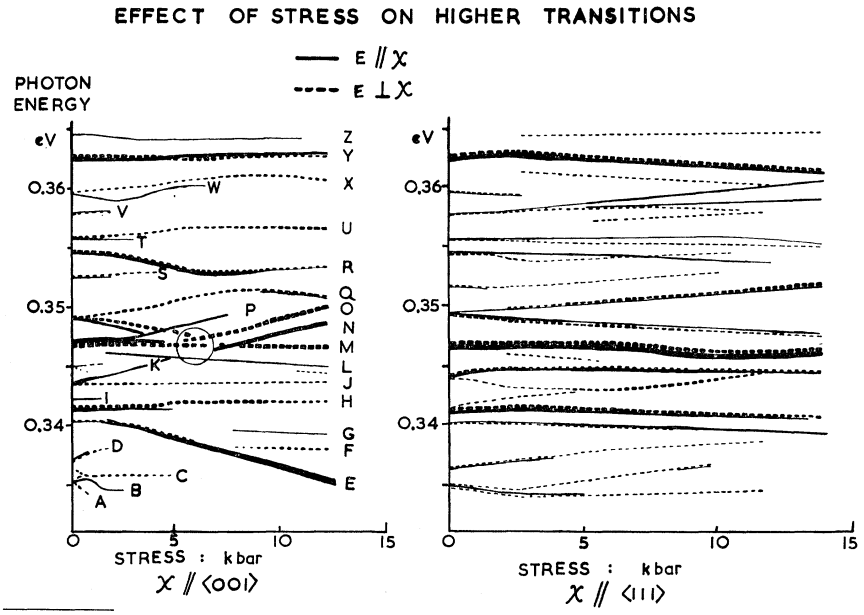

FIG. 4. The effect on the main acceptor spectrum of uniaxial stress along the two axes of highest symmetry. Width of lines represents the approximate intensity of the transition concerned, in the experimental spectra. In the ⟨001⟩ spectra, there are large changes of intensity under stress, and it is not always possible to be completely certain from which zero-stress component each high-stress component derives. A region of particular confusion through overlapping of absorption bands has been marked by a circle. Note the relatively stronger recoupling under ⟨001⟩ compression, where some of the letters refer to transitions identified in Table III.

[21] A. R. Goodwin and S. D. Smith (private communication).

kbar hydrostatic pressure would produce 1% change in phonon energy for diamond, compared with only the required 1.6 kbar calculated for lead.[22]

4. DISCUSSION

A. General

The effective-mass theorem, applied to shallow single-hole bound impurity states, implies that such a state may be usefully described by a "product wave function" taking the form:

$$\Phi(\mathbf{r})=\sum_j \phi_j(\mathbf{r})F_j(\mathbf{r})\,, \tag{1}$$

where the ϕ_j are a set of free-hole–band wave functions and the F_j are "envelope" wave functions varying more smoothly over atomic distances.[15]

Crucial to this theory, which through the *envelope* functions generates an analogy with hydrogenic theory, is the concept of the inverse mass. In general, for crystals, this quantity is not a simple scalar, but a tensor. It is defined as

$$C_{ts}{}^{\alpha\beta}=\frac{\partial}{\partial k_\alpha}\frac{\partial}{\partial k_\beta}W_{ts}(\mathbf{k})\,. \tag{2}$$

For the present purposes, since one is dealing exclusively with *hole* states, $W_{ts}(k)$ will be defined as the matrix element of the pure crystal hamiltonian between the free *hole* states $\phi_t(\mathbf{r})\exp(i\mathbf{k}\cdot\mathbf{r})$ and $\phi_s(\mathbf{r})\exp(i\mathbf{k}\cdot\mathbf{r})$, with the wave vector $\mathbf{k}$ small.

For the class-4 semiconductors C, Si, Ge the valence-band edge at the Γ point in the absence of spin-orbit interaction is the threefold degenerate $\Gamma_5{}^+(\Gamma_{25'})$ state belonging to the $O_h{}^{(7)}$ space group. Spin-orbit interaction splits the $\Gamma_5{}^+$ into two levels according to the familiar scheme $\Gamma_5{}^+\times D_{1/2}=\Gamma_7{}^+ + \Gamma_8{}^+$, where the resulting states are sometimes described also as $p_{1/2}, p_{3/2}$, respectively.

The $\Gamma_5{}^+$ inverse-mass tensor between the *spinless* wave functions has a symmetry such that its only non-vanishing components are

$$\begin{aligned} C_{xx}{}^{xx} &= (\hbar^2/m_0)L = \text{c.p.}\,,\\ C_{yy}{}^{xx}=C_{xx}{}^{yy} &= (\hbar^2/m_0)M = \text{c.p.}\,,\\ C_{xy}{}^{xy}=C_{yx}{}^{xy} &= (\hbar^2/m_0)N = \text{c.p.}\,, \end{aligned} \tag{3}$$

where m_0 is the free-electron mass, and allowing for cyclic permutation of cubic axes (c.p.). Note that according to the present definition of the effective mass, the parameters L, M, are essentially *positive* for a normal valence band at $\mathbf{k}=0$. The sign of L, M, N is inverted with respect to the parameters of Dresselhaus *et al.*[23]

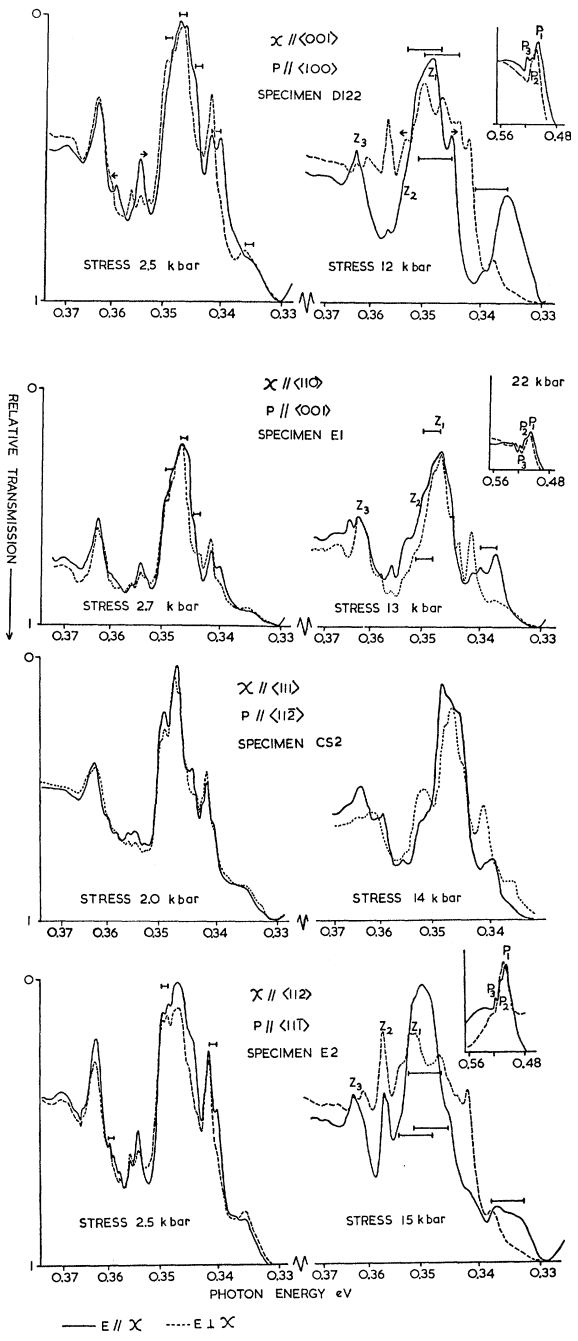

FIG. 5. The main acceptor spectrum under different uniaxial compressions. The same convention for polarization holds as for Fig. 3. Inserts refer to phonon-assisted transitions discussed in text.

It has been found that for silicon and germanium, many of the acceptor states possess envelope wave functions of sufficient spatial extent for the acceptor-hole potential energy to be taken as $V(r)=e/\kappa r$, where e= electronic charge, and r the radius out from the acceptor nucleus, κ is the dielectric constant. This result lends itself to the hydrogenic analogy, from which it is

[22] A. A. Maradudin, Phys. Status Solidi **2**, 1493 (1962).
[23] G. Dresselhaus, A. F. Kip, and C. Kittel, Phys. Rev. **98**, 368 (1955).

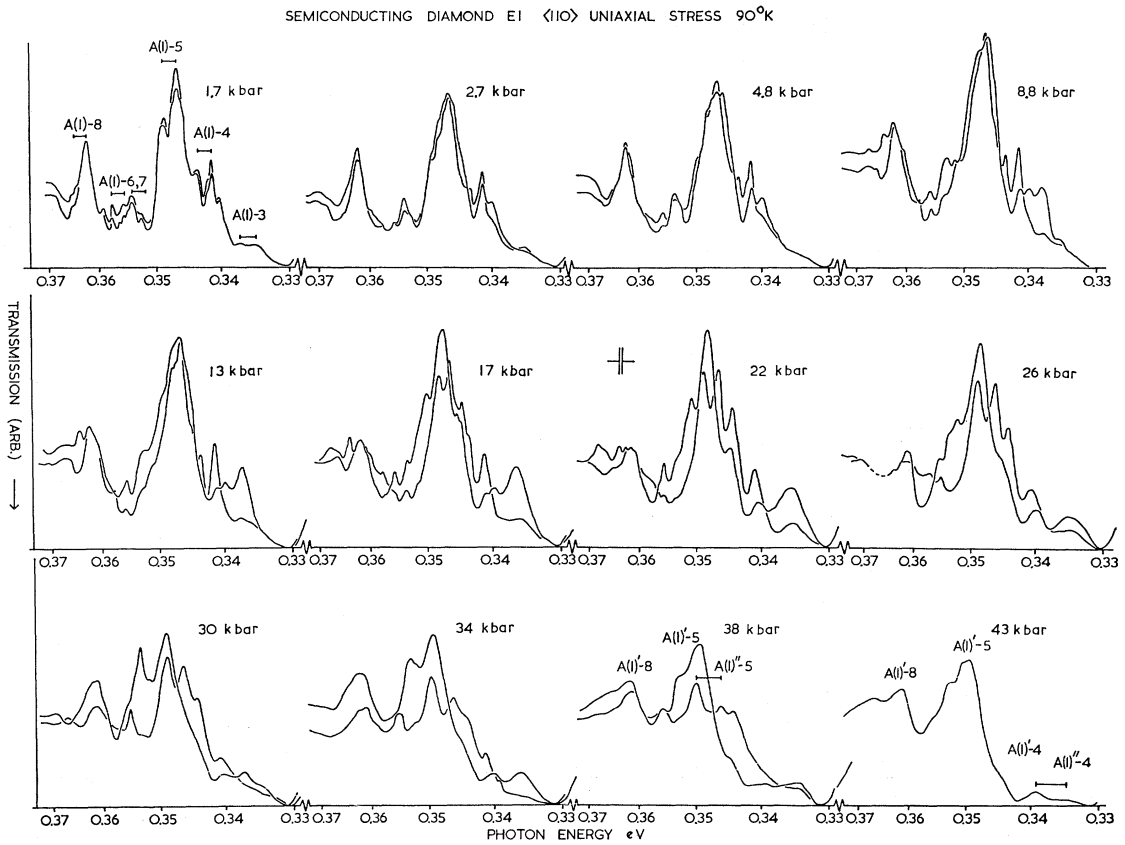

FIG. 6. The ⟨110⟩ compression spectra over the complete range of stresses covered. The convention for polarizations is that the $\mathbf{E}\|\chi$ component is shown continuous, the $\mathbf{E}\perp\chi$ disjointed. Note the large intensity changes and tendency to simplification under high stress.

expected that the lowest acceptor absorption bands should represent transitions between *s*- and *p*-like states.

There are two sources of *splitting* of these hydrogen-like states, the first being that the free band edge suffers spin-orbit splitting large relative to the splitting in atomic hydrogen. The second cause is the departure of the inverse mass tensor from spherical (scalar) symmetry of $L=M$, $N=0$, which may be described as *band-envelope* interaction.

For silicon and germanium, the free-band spin-orbit interaction is much stronger than the *band-envelope* interaction, so that the acceptor states there involve band wave functions remaining essentially coupled by the former. This is not true for diamond, where the free-band spin-orbit splitting is only 0.006 eV,[13] which makes such a simplification as described impossible.

Published band structures[24] show a consensus of opinion that for diamond in the present nomenclature $L>M$, $N>0$. It is also apparent that the departure from spherical symmetry is sufficient for it to be possible to interpret most of the experimental spectrum up to 0.3471 eV as involving predominantly *p*-like excited states.

In dealing with the group-theoretic classification of free-band states at the Γ point ($\mathbf{k}=0$)—associated point-group O_h—the established notation of Bethe,[25] employing parity symbols + and − has been used throughout. In order to achieve the maximum logical consistency with this nomenclature, a symbolism for the acceptor (T_d) point group has been used as defined by the character table given here (Table III). Since the T_d group is a subgroup of O_h, any representation of O_h is a representation of T_d. It will be observed that according to the nomenclature of Table III there is the simple $1\rightarrow 1$ relation on going from O_h to T_d of $\Gamma_{i^+}\rightarrow\Gamma_i$ ($i=1\cdots 7$). Note that the present nomenclature differs slightly from that previously used for silicon,[26,14] in that the Γ_4 and Γ_5 are interchanged.

$2p$ envelopes belong to the D_1 representation of the spherical group $D_{\infty h}$. The total splitting of the $2p$-like

[24] F. Herman, in *Proceedings of the Seventh International Conference on the Physics of Semiconductors, Paris, 1964* (Academic Press Inc., New York, 1965), p. 3; L. Kleinman and J. C. Phillips, Phys. Rev. **116**, 880 (1960); H. A. Kellner, Acta Physica Austriaca **18**, 48 (1964); W. Saslow, T. K. Bergstresser, and M. L. Cohen, Phys. Rev. Letters **16**, 354 (1966).

[25] H. Bethe, Ann. Physik **3**, 133 (1929).

[26] G. Dresselhaus, Phys. Rev. **100**, 582 (1955).

TABLE III. Group characters of the T_d double group. The nomenclature of the present paper differs slightly from that of Schechter (Ref. 14).

	E	$\bar{E}$	$8C_3$	$8\bar{C}_3$	$3C_2,3\bar{C}_2$	$6S_4$	$6\bar{S}_4$	$6\sigma_d,6\bar{\sigma}_d$
Γ_1	1	1	1	1	1	1	1	1
Γ_2	1	1	1	1	1	−1	−1	−1
Γ_3	2	2	−1	−1	2	0	0	0
Γ_4	3	3	0	0	−1	1	1	−1
Γ_5	3	3	0	0	−1	−1	−1	1
Γ_6	2	−2	1	−1	0	$\sqrt{2}$	$-\sqrt{2}$	0
Γ_7	2	−2	1	−1	0	$-\sqrt{2}$	$\sqrt{2}$	0
Γ_8	4	−4	−1	1	0	0	0	0

level in the crystal goes according to following scheme:

$$\Gamma_5^+ \times D_1^- \times D_{1/2} = 2\Gamma_6 + \Gamma_7 + 3\Gamma_8, \tag{4}$$

where $D_{1/2}$ represents the hole spin, and the right-hand side the six resulting split-off p-like levels. Since the band-envelope interaction predominates over the spin-orbit interaction in diamond, it is appropriate to introduce a *coupling scheme* into the above, thus we have

$$\Gamma_5^+ \times D_1^- = \Gamma_1 + \Gamma_3 + \Gamma_4 + \Gamma_5, \tag{5a}$$

$$\begin{aligned} &\Gamma_1 \times D_{1/2} = \Gamma_6(1),\ \Gamma_3 \times D_{1/2} = \Gamma_8(3), \\ &\Gamma_4 \times D_{1/2} = \Gamma_6(4) + \Gamma_8(4),\ \Gamma_5 \times D_{1/2} = \Gamma_7(5) + \Gamma_8(5). \end{aligned} \tag{5b}$$

In the above scheme, the primary band-envelope interaction produces the four spinless sublevels (5a). Spin-orbit interaction subsequently further splits two of these sublevels. In (5b) and subsequent such schemes, brackets are used to denote parent states. This coupling is the opposite of that used by Schechter for silicon.[14]

According to effective-mass theory, the crystal-field splitting of the spinless $2p$-like states is determined by the parameters L, M, and N. The expectation energies of the four are found to be, theoretically,

$$\begin{aligned} &\Gamma_1 : E_1 = -(5/4)(3L+2M+2N)^{-1}R_A, \\ &\Gamma_3 : E_3 = -(5/4)(3L+2M-N)^{-1}R_A, \\ &\Gamma_4 : E_4 = -(5/4)(L+4M-N)^{-1}R_A, \\ &\Gamma_5 : E_2 = -(5/4)(L+4M+N)^{-1}R_A, \end{aligned} \tag{6}$$

where R_A is the diamond acceptor Rydberg, defined as $R_A = R_\infty/\kappa^2 \approx 0.4$ eV. More refined estimates of the binding energy may be obtained by investigating the effect of weak admixture of non $2p$-like wave functions, by action of the nonspherical symmetry of mass. However, for diamond, such an investigation is unlikely to be of significance on its own, since the assumption of a centro-symmetric potential field is unlikely to be better than a rough approximation, on account of the relatively compact envelopes encountered in this material. From the ordering of L, M, N mentioned above, it would appear likely that the Γ_1 should be the least, and the Γ_4 the most strongly bound level. It is also likely that the Γ_3 is the second most strongly bound $2p$-like level. In the same way, the ground $1s$-like level, which is split only by spin-orbit interaction and is of symmetry $\Gamma_5 \times D_{1/2} = \Gamma_7(g) + \Gamma_8(g)$, has an expectation energy of $-E_A = -3(L+2M)^{-1}$.

The spin-orbit splitting predicted by simple effective-mass theory for the $2p$-like states is one-half the free-band splitting for the Γ_4 and Γ_5 derived levels, with the $\Gamma_8(4)$ bound more strongly than the $\Gamma_6(4)$, and the $\Gamma_8(5)$ less strongly than the $\Gamma_7(5)$:

$$E_8(5) - E_7(5) = E_6(4) - E_8(4) = \Delta/2. \tag{7}$$

It has been found possible to interpret the effects of stress only if it is assumed that the 2.1-meV ground-state splitting *is* the spin-orbit splitting of the ground Γ_5 state. That this differs considerably from the 6-meV free-band splitting is not thought serious, in view of the fact that the two would only be equal for a *pure* $1s$ ground state and that the effective-mass approximation is very unlikely to be accurate for the ground state, which has a "Bohr radius" of ~4 Å. The stress results are favorable to assigning to the ground-state splitting the same *sign* as for the free-hole splitting, namely with the Γ_8 below the Γ_7. This assignment is apparently at odds with the relative intensities of transitions at 70°K, since it is predicted that, except for the $\Gamma_7(5)$ band, all $2p$ excited levels should have a transition from the (lower) $\Gamma_5(g)$ ground state of intensity *greater* than that from the $\Gamma_7(g)$ state; whereas this is not apparent in the experimental spectra. Nevertheless, we have evidence from the stress work on the isolated 0.3042-eV transi-

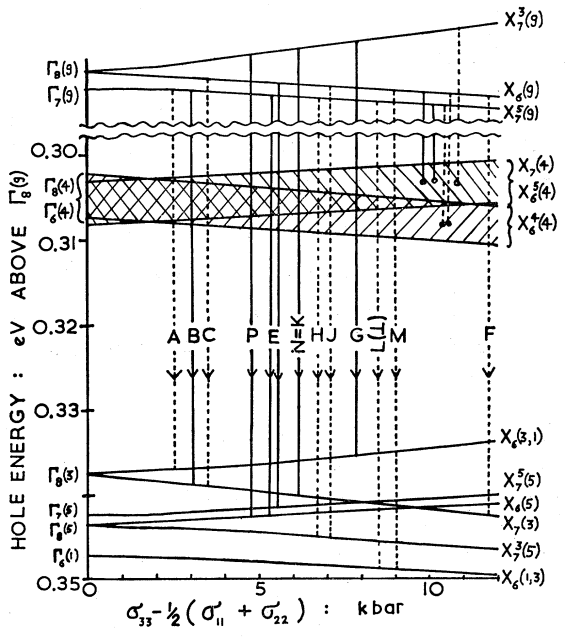

FIG. 7. A theoretical interpretation of the ⟨001⟩ compression spectra of Figs. 5 and 6, on the basis of transitions being between states with predominantly $1s$-$2p$-like envelopes. The hatched region represents the broad lowest excited-state region. For details see text and Table III.

tion (Sec. 3), for the extreme sensitivity of transition moments to only small shifts in energy. A further point *in favor* of the assignment lies in the fact that the fourfold degeneracy of the $\Gamma_8(g)$ state is twice that of the $\Gamma_7(g)$. On this population basis, the increase in intensity of nonquenched spectral components upon cooling to 4°K mentioned in Sec. 3 should be in the ratio 3:2 for a Γ_8, but 3:1 for a Γ_7 lower ground state. Reported experimental results are close to the former for bands involving a clear-cut division.[11]

Through combination of the thermal data with the present stress results, it has been possible to assign all the theoretical ground$\rightarrow 2p$-like transitions in the experimental spectrum, as shown in column (3) of Table I. It may be seen that this scheme is in full agreement with the theoretical predictions regarding ordering of levels discussed above [Eqs. (6), (7)], and classifies all the lowest observed transitions. Note that the transition interpreted as $\Gamma_7(g)\rightarrow\Gamma_7(5)$, which is forbidden by group theory, *appears* as a weak shoulder at 0.3404 eV. The explanation of this may be that the transition is allowed through the effect of local strains, which weakly destroy the ideal T_d acceptor symmetry. In order to explain the complicated shape and temperature behavior of the strong absorption band near 0.347 eV, we have also postulated (Table I) the existence of one additional non-$2p$-like Γ_7 level denoted by $\Gamma_7(2)$.

The broad lowest 0.3042-eV acceptor transition has been assigned to transitions to spin-orbit split Γ_4 p levels, $\Gamma_6(4)$ and $\Gamma_8(4)$, which are expected to have a splitting of the order of 3 meV [Eq. (7)]. Such a level splitting is consistent with the fact that the splitting of the transition is not detected, on account of its breadth of $\sim$6 meV.

B. Stress Effects

The experimental results have been interpreted on the basis that the effect of stress on acceptor states is due predominantly to induced perturbations of the valence-band edge. Symmetry arguments show that the matrix elements of the stress perturbation between the free-band spinless *electron* states at the Γ point are determined by three deformation parameters as follows:

$$W_{ij}(S)=\begin{bmatrix} D\sigma+K(2\sigma_{xx}-\sigma_{yy}-\sigma_{zz}) & 3E\sigma_{xy} & 3E\sigma_{xz} \\ 3E\sigma_{yx} & D\sigma+K(2\sigma_{yy}-\sigma_{zz}-\sigma_{xx}) & 3E\sigma_{yz} \\ 3E\sigma_{zx} & 3E\sigma_{zy} & D\sigma+K(2\sigma_{zz}-\sigma_{xx}-\sigma_{yy}) \end{bmatrix} \begin{matrix}(\varphi_x)\\(\varphi_y),\\(\varphi_z)\end{matrix} \tag{8}$$

where σ_{ij} is the stress tensor regarded as positive for compression, with a hydrostatic component $\sigma=\sigma_{xx}+\sigma_{yy}+\sigma_{zz}$. The parameters D, K, E represent the valence-electron lattice interaction of the diamond and are, related to the deformation potentials of Kleiner and Roth[27] as follows:

$$\begin{aligned} D_d{}^v&=(C_{11}+2C_{12})D,\\ D_{u'}{}^v&=\tfrac{3}{2}(C_{11}-C_{12})K,\\ D_u{}^v&=3C_{44}E, \end{aligned} \tag{9}$$

where the C_{ij} are the elastic constants in standard condensed notation. Note that the term in D is purely hydrostatic: It affects all valence-band states alike, and therefore should not affect the shift of acceptor transitions under stress. This is in accord with experimental results for hydrostatic stress. Within the effective-mass approximation, the stress-preturbation matrix element between the effective-mass states

$$\Phi=\sum_j \phi_j F_j \quad\text{and}\quad \Psi=\sum_j \psi_j G_j$$

of the Eq. (1) type is given by

$$\langle\Phi|W(S)|\Psi\rangle=\sum_{ij}\langle F_i|G_j\rangle\langle\phi_i|W(S)|\psi_j\rangle. \tag{10}$$

In general, recoupling of split $2p$-like excited states takes place under uniaxial stress.

⟨001⟩ Stress

There is strong recoupling of states in the ⟨001⟩ stress spectra. The effect of ⟨001⟩ stress is to reduce the acceptor symmetry from T_d to D_{2d}. The D_{2d} group irreducible representations used here are as defined by Koster.[28]

Under *weak* stress, the reduction of symmetry leads to the following splittings of the zero-stress–coupled ground and $2p$ excited states:

$$\begin{aligned} &\Gamma_8(g)\rightarrow X_6(g)+X_7{}^8(g), && \Gamma_7(g)\rightarrow X_7{}^7(g)\\ &\Gamma_8(4)\rightarrow X_6{}^8(4)+X_7(4), && \Gamma_6(4)\rightarrow X_6{}^6(4)\\ &\Gamma_8(3)\rightarrow X_6(3)+X_7(3), && \\ &\Gamma_8(5)\rightarrow X_6(5)+X_7{}^8(5), && \Gamma_7(5)\rightarrow X_7{}^7(5)\\ &\Gamma_6(1)\rightarrow X_6(1). && \end{aligned} \tag{11}$$

With higher stress, there is a tendency to recoupling of states. Complete recoupling of relevant states may occur where the stress perturbation is much greater than their zero-stress splittings. Because of their isolation, the Γ_4 levels do not appreciably recouple with other $2p$-like states over the range of stress practically available. A further simplification for ⟨001⟩ stress is that none of the Γ_5 derived $2p$-like states interact with the Γ_1 or Γ_3 derived states. The $X_6(3)$ low-stress level interacts and recouples with the $X_6(1)$ under high

[27] W. H. Kleiner and L. M. Roth, Phys. Rev. Letters **2**, 335 (1959).

[28] G. F. Koster, Solid State Phys. **5**, 173 (1957).

TABLE IV. ⟨001⟩ $1s$ and upper $2p$ hole states under low and high compressive stress. Shift rates are for *hole* states and are of opposite sign to the shift of the electron level itself. Hole energies are given relative to the lower ground state. The final column gives the theoretical intercepts; for comparison with experiment, see Table VI. Subscripts denote associated irreducible representations of T_d or D_{2d}; brackets denote parent spinless T_d states; superscripts denote parent states for a particular coupling. States which do *not* interact with others under ⟨001⟩ stress are denoted by an asterisk.

State	Shift rate	Actual origin (eV)	Extrapolated origin (eV)
		Low-stress states	
$X_7^{(7)}(g)$	$-D$	$\Gamma_7(g)$: $E_7=0.0021$	
$X_7^{(8)}(g)$	$-D-K$	$\Gamma_8(g)$: $E_8=0$	
$^*X_6(g)$	$-D+K$	$\Gamma_8(g)$: $E_8=0$	
$X_7^{(8)}(5)$	$-D+\frac{1}{2}K$	$\Gamma_8(5)$: $E_8^{(5)}=0.3435$	
$X_7^{(7)}(5)$	$-D$	$\Gamma_7(5)$: $E_7^{(5)}=0.3421$	
$^*X_6(5)$	$-D-\frac{1}{2}K$	$\Gamma_8(5)$: $E_8^{(5)}=0.3435$	
$X_6(1)$	$-D$	$\Gamma_6(1)$: $E_6(1)=0.3471$	
$^*X_7(3)$	$-D+K$	$\Gamma_8(3)$: $E_8(3)=0.3373$	
$X_6(3)$	$-D-K$		
		High-stress recoupled states	
$X_7^{(3)}(g)$	$-D-2K$	$\Gamma_5(g)$: 0	$\frac{2}{3}E_8+\frac{1}{3}E_7=0.0007$
$X_7^{(5)}(g)$	$-D+K$	$\Gamma_7(g)$: 0.0021	$\frac{1}{3}E_8+\frac{2}{3}E_7=0.0014$
$X_7^{(3)}(5)$	$-D+K$	$\Gamma_8(5)$: 0.3435	$\frac{2}{3}E_8(5)+\frac{1}{3}E_7(5)=0.3430$
$X_7^{(5)}(5)$	$-D-\frac{1}{2}K$	$\Gamma_7(5)$: 0.3421	$\frac{1}{3}E_8(5)+\frac{2}{3}E_7(5)=0.3426$
$X_6(3,1)$	$-D-2K$	$\Gamma_8(3)$: 0.3373	$\frac{2}{3}E_8(3)+\frac{1}{3}E_6(1)=0.3406$
$X_6(1,3)$	$-D+K$	$\Gamma_6(1)$: 0.3471	$\frac{1}{3}E_8(3)+\frac{2}{3}E_6(1)=0.3438$

stress. Group theoretically, the recoupled Γ_1, Γ_3, Γ_5 derived excited levels and the ground levels may be obtained by reduction of the sum of the relevant *spinless* T_d representations into *spinless* representations of D_{2d} *prior* to applying spin-orbit interaction as a secondary perturbation, thus

$$\begin{aligned}
&\Gamma_5(g)=X_3(g)+X_5(g);\ X_3(g)\times D_{1/2}=X_7^3(g),\\
&\qquad X_5(g)\times D_{1/2}=X_6(g)+X_7^5(g),\\
&\Gamma_1+\Gamma_3=2X_1+X_2;\ 2X_1\times D_{1/2}=X_6(1,3)+X_6(3,1),\\
&\qquad X_2(3)\times D_{1/2}=X_7(3),\\
&\Gamma_5=X_3(5)+X_5(5);\ X_3(5)\times D_{1/2}=X_7^3(5),\\
&\qquad X_5(5)\times D_{1/2}=X_6(5)+X_7^5(5).
\end{aligned} \tag{12}$$

In these decompositions, brackets and superscripts are used to distinguish levels of the same symmetry (subscript). The form of the actual recoupling process is illustrated in Fig. 7.

Table IV shows the theoretical shift rates and zero-stress origins for the $1s$ and $2p$ hole states under ⟨001⟩ compression; the detailed analysis of the polarization shift rates of the zero-phonon acceptor spectrum under ⟨001⟩ stress is presented in Table V. Theoretical shift rates have been determined throughout by Eq. (10). When recoupled under high stress, resulting levels then in theory regain *linear* shift rates with stress. Also, if the high-stress recoupled levels one *extrapolated* back to zero stress, their intercepts are completely determined by the positions of the *actual* zero-stress levels, although not in general coincident with them. Theoretical values of shift rates, actual origins, and extrapolated zero-stress intercepts of levels under strong ⟨001⟩ recoupling are given in Table V, where the zero-stress matrix element of energy have been chosen to fit the assignment given in Table I to the experimental zero-stress spectra. Thus the consistency of this assignment has been checked against the stress effects in Table V.

The selection rules in Table V are divided into two columns. In the first are those derived from simple $s\rightarrow p$ effective-mass theory. These are often more restrictive than those derived solely from group theory, which are shown in the second column. Examination of Table V shows that the simple effective-mass selection rules are in general a good guide. Comparison of the experimental and theoretical sides of Table V shows good agreement in the actual and extrapolated origins of most transitions. As mentioned in Sec. 3, the *actual* origins of a few high-stress transitions are obscured somewhat by the merging of bands at intermediate stress. Note that the fact that the weak shoulder at 0.3399 eV appears in Fig. 4 to contribute to the strong high-stress band E, which is not accounted for on the simple theory used for Table V, is probably due to the same cause, random strain, used in Sec. 4A to explain the existence of the shoulder at zero stress. The ⟨001⟩ stress spectra, because of their relative simplicity, have been of particular value in assigning the zero-stress transitions of Table I.

Interpretation of the stress-perturbed 0.3042-eV band is complicated by its great breadth. Under high-stress recoupling, the $2p$ Γ_4-derived states are expected to split into three (overlapping) levels: $X_7(4)$ and $X_6^5(4)$, both with shift rate $-D-\frac{1}{2}K$, and $X_6^4(4)$ with shift rate $-D+K$. Transitions to the Γ_4-derived states allowed under ⟨001⟩ and other directions of stress are shown with their shift rates in Tables V and VI.

TABLE V. The higher transitions under ⟨001⟩ stress. Character symbols are used as for Table IV. Transitions are labeled as in Fig. 7. Couplings are labeled as follows: H, both ground and excited states are stress recoupled M, ground state alone is recoupled; A, neither ground nor excited states are recoupled; L, neither ground nor excited states are recoupled. Nearly all transitions allowed by simple effective-mass theory have been detected Polarizations refer to the electric vector with respect to the stress direction. In cases where the coupling is changing over the range of stress concerned, the two limiting theoretical conditions are given on the right, and are separated by a solidus.

Component	Polarization of E	Range of stress where linear (kbar)	Experimental actual origin (eV)	Experimental extrapolated origin (eV)	Experimental shift rate (meV/kbar)	Experimental comment	Theoretical assignment	Coupling state	Simple selection rule for E	Suppl. selection rule for E	Theoretical actual origin (eV)	Theoretical extrapolated origin (eV)	Theoretical shift rate	Comment in light of theory
A	⊥	...	0.3355±10	...	<0	Rapidly lost	$X_7^{(2)}(g)-X_6(3)$	L	⊥(∥)	∥	0.3352	...	$-K$	
B	∥	>2?	?	0.3370±15	<0	Confused; rapidly lost	?	...	...	...	...	...	...	An unresolved mixture?
C	⊥	>2	?	0.3358±5	0.00±0.03	Lost at ~5 kbar	$X_7^{(3)}(g)-X_7(3)$	M	⊥	...	0.3352	0.3359	0	
D	⊥	...	0.3373±5	...	>0	Rapidly lost	$X_6(g)-X_7(3)$	A	⊥	...	0.3373	0.3373	0	Continuous with "F"?
$D(\parallel)$	∥	...	0.3373±10	...	>0	Very rapidly lost	$X_7^{(3)}(g)/X_7^{(3)}(g)-X_6(3)$	L/M	⊥=∥		0.3373	...	0/+K	Continuous with "G"?
E	∥(⊥)	>4	0.3402±3	0.3416±4	−0.43±0.02	Broad	$X_6(g)-X_7^{(3)}(5)$ $X_7^{(3)}(g)-X_6(5)$	H	∥	⊥	0.3421 0.3413	0.3426 0.3419	−¾K	0.7-meV split concealed by breadth: See text [Sec. 4]
F	⊥	>8	?	0.3385±15	−0.05±0.03	Appears ~8 kbar	$X_6(g)-X_7(3)$	A	⊥	∥	0.3373	0.3373	0	Continuous with $D(\perp)$,
G	∥	>9?	?	0.3400±10	−0.05±0.04	Appears on side of "E"	$X_7^{(3)}(g)-X_6(3)/X_6(3,1)$	M/H	∥	⊥	0.3373	0.3399	K/0	Continuous with "$D(\parallel)$," recoupled at 12 kbar.
H	⊥	>6	0.3415	0.3422±3	0.00±0.02		$X_7^{(3)}(g)-X_7^{(3)}(5)$	H	⊥	...	0.3415	0.3423	0	
J	⊥	all?	0.3435	0.3433±3	0.01±0.02	Weak	$X_6^{(3)}(g)-X_7^{(3)}(5)$	H	∥		0.3435	0.3430	0	
$L(\perp)$	⊥	?	?	?	??	Appears at 0.3448 eV at 12 kbar	$X_7^{(3)}(g)-X_6^{(1)}/X_6(1,3)$	M/H	⊥	∥	0.3450	0.3457/ 0.3424	0	Transition contributes also to $L(\parallel)$?
$L(\parallel)$	∥	>4	0.3463	0.3465±3	−0.11±0.03		$X_6(g)-X_7(2)$?	A	?,	∥, ⊥	0.3463	0.3463	$-K$	Excited state interacting,
N	∥	?	?	0.3435±10	0.42±0.04	Continuous with K?	$X_7^{(3)}(g)-X_6(5)$	H	⊥	∥	0.3435	0.3428	¾K	Polarization induced by mixing in excited state?
M	⊥	>5?	Ca 0.347	0.3472±4	−0.04±0.03	Rather broad	$X_6(g)-X_6(1)/X_6(1,3)$	M/H	⊥	...	0.3471	0.3471/ 0.3438	$-K$/0	Contains other components unresolved?
O	⊥	>8	Ca 0.347?	0.3448±8	0.45±0.03	Crossing other bands uncertain	$X_7^{(3)}(g)-X_7(2)$? $X_7^{(3)}(g)-X_6(1)/X_6(3,1)$	H M/H	⊥	...	0.3463	0.3456	2K	$\Gamma_1\Gamma_3$ not recoupled before line disappears.
P	∥	~5?		0.3458±8	0.38±0.06				∥/0	⊥/∥ ⊥	0.3471	0.3464/ 0.3431	2K/3K	

Other Directions of Stress

The ⟨111⟩ compression spectrum is seen to be more complicated experimentally than the ⟨001⟩. There is hardly any sign of complete recoupling up to 15 kbar. This is due in part to the fact that the Γ_5 derived excited levels now no longer refrain from interacting under stress with the Γ_1 and Γ_3 derived levels. The majority of fully recoupled $2p$ levels would thus emerge only at stresses sufficient to effect this, which requires larger shifts than are necessary in the ⟨001⟩ case. Also, ⟨111⟩ compression produces less splitting per applied stress than does ⟨001⟩ compression. It is expected theoretically that the effect of ⟨111⟩ compression upon transitions to the broad Γ_4 levels should be qualitatively similar to those obtaining for ⟨001⟩ compression, which is observed (Fig. 3).

Because of the steadily changing couplings in most of the acceptor spectrum under ⟨111⟩ stress, we have used from these spectra only results obtained from the isolated (Γ_4) 0.3042-eV band for quantitative estimation of the ⟨111⟩ deformation potential in Table VI. ⟨111⟩ compression reduces T_d site symmetry to C_{3v}, the nomenclature of which symmetry is taken from Koster.[28] *Qualitatively*, the ⟨111⟩ stress spectrum appears to be in general agreement with the proposed assignment of transitions.

For ⟨110⟩ compression, the situation is even more complicated still since the deformation now, in reducing T_d to C_{2v} symmetry, is capable of completely destroying spin-orbit coupling, in that at sufficiently high stress no spin-orbit *multiplets* exist. The C_{2v} characters are again taken from Koster, where σ_v is taken as reflection in the $(1\bar{1}0)$ plane.[28] Even though very high stresses were obtained in the ⟨110⟩ experiment (Fig. 6), full recoupling of some of the $2p$ states is believed incomplete at the highest stress obtained. There is a tendency under this deformation for some $2p$ levels, notably $\Gamma_6(1)$, to interact strongly with higher non-$2p$ levels *before* the $2p$-like states have completely recoupled between themselves.

⟨110⟩ compression is additionally complicated, since the resulting spectra are expected to be dependent upon the light propagation direction. This direction was close to the ⟨001⟩ for the present experiment. Polarization of transitions is along either ⟨001⟩, ⟨110⟩, or $\langle 1\bar{1}0\rangle$ axes for ⟨110⟩ compression. The $\mathbf{E}\|\langle 001\rangle$ components were therefore not detected strongly in the present experiment, and were rapidly lost under stress

Application of ⟨110⟩ stress is expected to lead to the following $2p$-like splittings at moderately high stress:

$$\Gamma_1+\Gamma_3+\Gamma_5=3\Sigma_1+\Sigma_2(3)+\Sigma_3(5)+\Sigma_4(5),$$
$$\Gamma_4=\Sigma_2(4)+\Sigma_3(4)+\Sigma_4(4), \tag{13}$$

while the ground states are split into three levels under stress:

$$\Gamma_5(g)=\Sigma_1(g)+\Sigma_3(g)+\Sigma_4(g). \tag{14}$$

TABLE VI. Spectral shift rates. All assignments used, except for the last two, are made for the high-stress recoupled states. Subscripts denote irreducible representations of the deformed point groups; while for ⟨001⟩ and ⟨111⟩ superscripts indicate spinless representations of the deformed groups from which they derive. Shift rates are given theoretically as the difference of excited-states minus ground-state shifts. The transitions used in the evaluation of the best fit ($K=0.262.10^{-6}$, $E=0.126.10^{-6}$ eV/kbar) are shown thus with an asterisk.

Stress direction	Expt. shift rate: 10^{-6} eV/kbar	Pol. of **E** vector	Transition	Theoretical shift rate, and best theoretical fit (10^{-6} eV/kbar)	
⟨001⟩	+0.14 unresolved	⊥	$\left\{\begin{matrix} X_7^{(3)}(g)-\left\{\begin{matrix} X_6^5(4) \\ X_7(4) \end{matrix}\right. \\ \left.\begin{matrix} X_6(g) \\ X_7^5(g) \end{matrix}\right\}-X_6^4(4) \end{matrix}\right.$	$(-\frac{1}{2}K)-(-2K)=\frac{3}{2}K$ $(K)-(K)=0$	0.393 0 } approx. 0.2?
	*−0.38±0.03	∥	$\left\{\begin{matrix} X_6(g)-X_7(4) \\ X_7^5(g)-X_6^5(4) \end{matrix}\right\}$	$(-\frac{1}{2}K)-(K)=-\frac{3}{2}K$	−0.393
	*+0.42±0.04	∥	$X_7^3(g)-X_6(5)$	$(-\frac{1}{2}K)-(-2K)=\frac{3}{2}K$	+0.393
	*−0.43±0.02	∥	$\left\{\begin{matrix} X_7^5(g)-X_6(5) \\ X_6(g)-X_7^5(5) \end{matrix}\right\}$	$(-\frac{1}{2}K)-(K)=-\frac{3}{2}K$	−0.393
	+0.45±0.03	⊥	$X_7^3(g)-X_7(2)$?	$0-(-2K)=2K$	+0.524?
⟨111⟩	+0.1±0.03 unresolved	⊥	$\left\{\begin{matrix} \left\{\begin{matrix} \Lambda_6^1(g)-\Lambda_{4,5}^3(4) \\ \Lambda_6^1(g)-\Lambda_6^3(4) \end{matrix}\right\} \\ \left\{\begin{matrix} \Lambda_{4,5}^3(g)-\Lambda_6^2(4) \\ \Lambda_6^3(g)-\Lambda_6^2(4) \end{matrix}\right\} \end{matrix}\right.$	$(-\frac{1}{2}E)-(2E)=\frac{3}{2}E$ $(E)-(E)=0$	+0.189 0 } approx. +0.1
	*−0.19±0.02	∥	$\left\{\begin{matrix} \Lambda_{4,5}^3(g)-\Lambda_{5,4}^3(4) \\ \Lambda_6^3(g)-\Lambda_6^3(4) \end{matrix}\right\}$	$(-\frac{1}{2}E)-(E)=-\frac{3}{2}E$	−0.189
⟨110⟩ stress	faint trace	∥	$\Sigma_1(g)-\Sigma_3(4)$	$(\frac{1}{4}K-\frac{3}{4}E)-K=-\frac{3}{4}K-\frac{3}{4}E$	−0.291
⟨011⟩∥ propagation	*−0.17±0.03	∥	$\Sigma_4(g)-\Sigma_2(4)$	$-\frac{1}{2}K(-\frac{1}{2}K+\frac{3}{2}E)=-\frac{3}{2}E$	−0.189
	0.02±0.03	⊥	$\left\{\begin{matrix} \Sigma_1(g)-\Sigma_4(4) \\ \Sigma_3(g)-\Sigma_2(4) \end{matrix}\right.$	$(\frac{1}{4}K+\frac{3}{4}E)-(K)=-\frac{3}{4}K+\frac{3}{4}E$ $-\frac{1}{2}K-(-\frac{1}{2}K-\frac{3}{2}E)=\frac{3}{2}E$	−0.100 } approx. +0.189 } 0.04
	unresolved	∥			
	*−0.314±0.04	∥	$\Sigma_1(g)-\Sigma_3(5)$	$(\frac{1}{4}K-\frac{3}{4}E)-(K)=-\frac{3}{4}K-\frac{3}{4}E$	−0.291
	*−0.186±0.02	∥	$\Sigma_4(g)-\Sigma_2(3)$	$-\frac{1}{2}K-(-\frac{1}{2}K+\frac{3}{2}E)=-\frac{3}{2}E$	−0.189
	*+0.301±0.03	∥	$\Sigma_3(g)-\Sigma_1(1)$	$0-(-\frac{1}{2}K-\frac{3}{2}E)=\frac{1}{2}K+\frac{3}{2}E$	+0.320
	*−0.211±0.03	⊥	$\Sigma_4(g)-\Sigma_1(5)$	$-\frac{1}{2}K-(-\frac{1}{2}K+\frac{3}{2}E)=-\frac{3}{2}E$	−0.189

In the above equations, the stress is taken as sufficient to destroy zero-stress spin-orbit coupling. Since no C_{2v} state may be split by spin-orbit coupling, no reference to the latter need be included in classification of C_{2v} states. In (13) the $\Sigma_2(3)$ level derives purely from the Γ_3 and does not interact, while the $\Sigma_3(5)$ and $\Sigma_4(5)$ derive from the Γ_5 level alone, and do not interact with other levels once spin-orbit interaction is broken. Of the three Σ_1 states, one is composed of Γ_1 and Γ_3 derive states, while the other two involve interaction of Γ_1, Γ_3, and Γ_5 derived states.

Several transitions under ⟨110⟩ stress have been identified in medium- and high-stress coupling. The most reliable of these are given in Table VI. ⟨110⟩ compression produces transition shift rates which depend on *both* the shear deformation potentials, and this provides a good check on the ⟨001⟩ and ⟨111⟩ experiments.

⟨110⟩ spectra taken for the 0.3042-eV component show a band sharpening effect for the $\mathbf{E}\perp\chi$, i.e., $\mathbf{E}\|\langle 1\bar{1}0\rangle$ component, where the band goes through a minimum width at about 20 kbar. Interpretation of this effect in terms of recoupling in the zero-stress "virtual" split in this transition shows that the phenomenon is consistent with the $2p$-Γ_4 spin-orbit splitting being ~3 meV, and favors putting the $\Gamma_8(4)$ level below the $\Gamma_6(4)$, in agreement with theory [Eq. (7)]. The existence of a component with $\mathbf{E}\|\chi$ in these spectra which appears to follow the main $\mathbf{E}\perp\chi$ component is thought to be associated with the slow decoupling of the Γ_4 spin-orbit levels.

⟨112⟩ compression reduces the symmetry still further to C_{1h}. Under this action, *polarizations* of some components are no longer defined completely by symmetries of states, but depend on the ratio of deformation parameters K/E. As a result, there is a depolarization of some splittings under stress, especially in the 0.3042-eV band (Fig. 3).

Table VI compares theory and experiment as regards shift rates for the experiments in the three principal stress directions. The Γ_4 derived states involved in the 0.3042-eV band are represented in the high-stress recoupling condition throughout. This band splits to produce only one shift rate for $\mathbf{E}\|\chi$, which has been used in the table. Because of the breadth of the band, although more than one shift rate for $\mathbf{E}\perp\chi$ may be induced under stress, such components have not been clearly resolved apart, and thus the $\mathbf{E}\perp\chi$ results for

this band have not been used in estimating the deformation parameters.

Fairly good agreement in shift rates is evident, and the best theoretical fit to all reliable results has been found to be

$$K=+2.62\pm0.2\times10^{-7}\text{ eV bar}^{-1},$$
$$E=+1.26\pm0.2\times10^{-7}\text{ eV bar}^{-1}.$$

These results indicate deformation potentials for the valence bands of

$$D_u{}^v=+2.47\pm0.2\text{ eV},$$
$$D_{u'}{}^v=+1.63\pm0.2\text{ eV},$$

where use has been made of the following elastic constants

$$C_{11}-C_{12}=0.63\times10^{13}\text{ dyn cm}^{-2},$$
$$C_{44}=0.43\times10^{13}\text{ dyn cm}^{-2}.$$

The deformation potentials so obtained agree in sign with those found by Hensel and Feher for *silicon* which are[29]

$$D_u{}^v=+2.04\text{ eV},$$
$$D_{u'}{}^v=+2.68\text{ eV}.$$

It is to be noted that the anisotropy factor, $D_u/D_{u'}$, is given as 1.4 for diamond compared with 0.76 for silicon.

One last remark in the light of the present assignment of transitions should be made on the weak-absorption peak detected at 0.268 eV in heavily doped *synthetic* diamonds.[30] Smith and Taylor[8] interpreted the breadth of the 0.3042-eV acceptor transition of natural diamond as being a lifetime broadening effect induced by rapid phonon relaxation of the excited state involved back to a lower state whose position they estimated at about 0.268 eV above the ground level.

It is consistent with their work to postulate that the 0.268-eV transition is to an upper state which is mainly s like—the transition is analogous to the forbidden $1s\rightarrow 2s$ hydrogen transition. The T_d diamond acceptor site does *not*, however, possess inversion symmetry, so that parity is not a proper quantum number of the system, but since simple effective-mass theory involves energy operators of only even parity, this theory still forbids the transition in question. Some departure from effective-mass theory is very likely in diamond, so that the appearance of the 0.268-eV transition is taken as evidence of the relaxation of "parity" derived selection rules. The high density of acceptors in the *synthetic* diamonds may also have the effect of enhancing the transition by local center-center interactions. It is known that impurity concentrations can be sufficiently high for production of an impurity band. The fact that the 0.268-eV level is depressed well below the $2p$-like levels suggests that it contains—in hydrogenic terms—strongly mixed envelope wave functions, mainly of even parity.

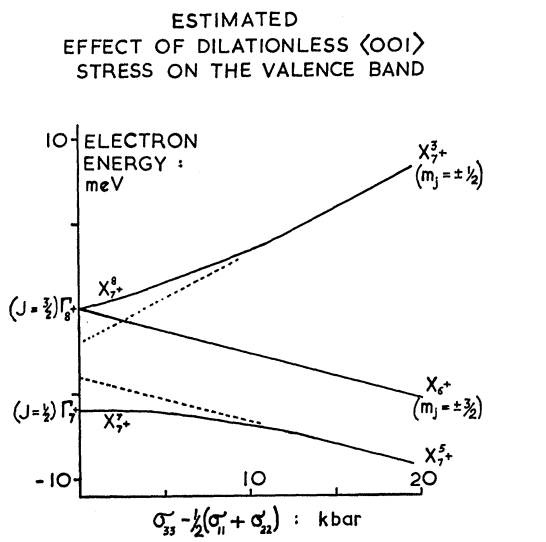

FIG. 8. The effect of ⟨001⟩ compression on the diamond free valence-band edge, *calculated* from the present experiments. The reduction of symmetry is from the associated point group $O_h\rightarrow D_{4h}$. Symbols denote irreducible representations of these groups associated with each level. The D_{4h} symbols have been chosen so that $X_i{}^+$ corresponds to X_i of D_{2d} (Table IV) for all D_{2d} operations. The angular momentum symbols derived by analogy with atomic theory correspond to those employed in Ref. (28). Superscripts refer to parent O_h or D_{4h} states in the limits of low- or high-stress coupling, respectively.

5. SUMMARY AND CONCLUSIONS

After examination of the stress experiments in terms of effective-mass theory, it has been possible to advance a reasonable scheme for the classification of the lowest 12 diamond acceptor transitions. The effects of stress along different directions have been shown to be consistent in the main with this scheme, and further recourse to effective-mass theory has enabled estimates to be made of the valence-band deformation potentials. The estimated effect of ⟨001⟩ stress upon the valence-band edge thus obtained is shown in Fig. 8.

Some deviations from effective-mass theory predictions have been detected, and it would be of interest to compare the present estimates of the deformation potentials with measurements of these obtained by other means. As far as we are aware, none exist at present for diamond. There is some reason to believe that the potentials obtained here *underestimate* effects in the free band.[31]

[29] J. C. Hensel and G. Feher, Phys. Rev. **129**, 1041 (1963). These experiments have been reinterpreted by Balslev and Lawaetz, Phys. Letters **16**, 6 (1965) according to whom the silicon deformation potentials are $D_u{}^v=+3.4$, $D_{u'}{}^v=+4.4$ eV. See also I. Balslev, Phys. Rev. **143**, 636 (1966).

[30] A. T. Collins, P. J. Dean, E. C. Lightowlers, and W. F. Sherman, Phys. Rev. **140**, A1272 (1965).

[31] J. J. Hopfield (private communication).

It would also be of interest to compare the classification of states and the stress effects with the effect of very strong magnetic fields upon the spectrum. The present authors have conducted experiments with fields up to 21 kOe, and the observed effects were consistent with effective mass $m^* \sim m_0$, but they indicated that fields of $\gtrsim 100$ kOe are required for well-resolved splittings. Such experiments have recently been undertaken.[32]

[32] D. M. S. Bagguley and G. Vella-Coleiro (private communication).

PHYSICAL REVIEW VOLUME 154, NUMBER 3 15 FEBRUARY 1967

Faraday Rotation in ZnO: Determination of the Electron Effective Mass

W. S. Baer
Bell Telephone Laboratories, Murray Hill, New Jersey
(Received 9 August 1966)

The electron effective mass in ZnO has been determined from free-carrier Faraday rotation. A value of $0.24m_0$ is obtained for the high-frequency band mass, giving a value of $0.29m_0$ for the low-frequency polaron mass. The free-carrier Faraday rotation in a polar compound is well described by a simple Drude theory, although polaron corrections may be important to other optical properties. The interband Faraday rotation in ZnO agrees with theoretical models assuming direct transitions between parabolic valence and conduction bands.

INTRODUCTION

OPTICAL studies[1,2] have shown ZnO to be a direct-gap semiconductor with a single s-like conduction-band minimum at the center of the Brillouin zone. Although this band structure is well established, a number of experiments have given disparate values for the electron effective mass. Measurement of shallow-donor binding energies by Hutson[3] yields a mass of about 0.27 times the free-electron mass, while the exciton binding-energy results of Thomas[1] combined with analysis of the shape of the absorption edge by Dietz, Hopfield, and Thomas[2] give a higher value near 0.38. A different interpretation of the exciton data by Park, Litton, Collins, and Reynolds[4] results in a reduced exciton mass ratio $\mu/m_0=0.20$.

The above experiments determine a low-frequency electron effective mass. Since ZnO is a polar compound, one must distinguish between measurements made at frequencies above and below the highest longitudinal optical phonon frequency which occurs at 590 cm^{-1} or 17 μ in ZnO.[5] The low-frequency polaron mass should be larger than the high-frequency bare mass because of coupling of the electron to the longitudinal optical phonons. In ZnO this polaron correction should be, at most, 20%. A determination of the high-frequency electron effective mass was made by Collins and Kleinman,[5] who measured the reflectivity from a ZnO crystal containing 5×10^{18} carriers and applied a Drude-type analysis to the free-electron contribution to the optical constants. Collins and Kleinman reported an effective-mass ratio of 0.06, which is too low to be consistent with the low-frequency results. Recent reflectivity data from $SrTiO_3$,[6] however, suggest that a classical Drude theory may not be adequate to describe free electrons in a polar compound. It may be necessary to calculate polaron contributions to the optical constants in some detail rather than include them in a small effective-mass correction.

Faraday rotation permits an independent measurement of the high-frequency electron effective mass and a test of the Drude theory at high frequencies. Under the conditions $\omega_g > \omega \gg \omega_l$ and $\omega \gg 1/\tau$, where ω is the radiation frequency, $\hbar\omega_g$ the semiconductor band-gap energy, ω_l the longitudinal optical phonon frequency, and τ the electron relaxation time, the interband and free-carrier Faraday rotations should be additive, with the free-carrier rotation displaying a Drude ω^{-2} or λ^2 dependence. This paper reports such results in ZnO and a determination of the electron effective mass in best agreement with that from donor binding-energy measurements.[3] In addition, the interband Faraday rotation is compared with two current theoretical models.

[1] D. G. Thomas, J. Phys. Chem. Solids **15**, 86 (1960).
[2] R. E. Dietz, J. J. Hopfield, and D. G. Thomas, J. Appl. Phys. **32**, 2282 (1961).
[3] A. R. Hutson, J. Appl. Phys. **32**, 2287 (1961); Phys. Rev. **108** 222 (1957).
[4] Y. S. Park, C. W. Litton, T. C. Collins, and D. C. Reynolds, Phys. Rev. **143**, 512 (1966).
[5] R. J. Collins and D. A. Kleinman, J. Phys. Chem. Solids **11**, 190 (1959).
[6] A. S. Barker, in *Proceedings of the International Colloquium on Optical Properties and Electronic Structure of Metals and Alloys, Paris, 1965* (North-Holland Publishing Company, Amsterdam, 1965).